Science of the Total Environment 634 (2018) 1192–1204

Contents lists available at ScienceDirect

Science of the Total Environment

journal homepage: www.elsevier.com/locate/scitotenv

Trends in heterogeneous aqueous reaction in continuous haze episodes in suburban Shanghai: An in-depth case study

Lingdong Kong *, Chengtian Du, Assiya Zhanzakova, Tiantao Cheng, Xin Yang, Lin Wang, Hongbo Fu, Jianmin Chen *, Shicheng Zhang

Shanghai Key Laboratory of Atmospheric Particle Pollution and Prevention, Institute of Atmospheric Sciences, Department of Environmental Science & Engineering, Fudan University, Shanghai 200433, China

HIGHLIGHTS

- Increasing trend of nitrate aerosol pollution in haze episodes
- Particulate liquid water plays important roles in formation of secondary aerosols.
- Secondary aerosols are main sources of haze.
- The occurrence of heterogeneous aqueous reaction has a marked tendency.
- High-nitrate haze episode favoured heterogeneous aqueous oxidation of SO_2.

GRAPHICAL ABSTRACT

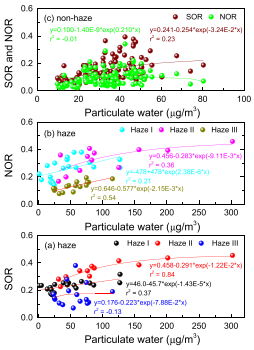

ARTICLE INFO

Article history:
Received 6 December 2017
Received in revised form 3 April 2018
Accepted 6 April 2018
Available online 18 April 2018

Editor: Lidia Morawska

Keywords:
Heterogeneous aqueous reaction
Secondary aerosol
Haze
Particulate liquid water

ABSTRACT

Heterogeneous aqueous reaction plays important roles in the enhanced formation of secondary aerosols during haze. However, its occurrence in haze episodes remains poorly understood. In this study, the trends in heterogeneous aqueous reaction in continuous haze episodes were investigated by an in-depth case analysis. The highly time-resolved measurements of water-soluble inorganic ions of $PM_{2.5}$ were conducted in a suburban of Shanghai, China, and continuous haze episodes, which occurred from Feb. 18 to Feb. 28, were selected as studied cases. Results showed that fine particle pollution in Baoshan was serious. High concentrations of secondary inorganic aerosol ions and the higher sulfur oxidation ratio (SOR) and nitrogen oxidation ratio (NOR) on haze days indicated enhanced conversions from SO_2 and NO_x to their corresponding particulate phases. The high-nitrate haze episode and the high-sulfate haze episode were identified. Further simulations revealed that the $PM_{2.5}$ particles had strong acidity during the high-nitrate and high-sulfate haze episodes whether they were calculated by E-AIM 4 or by ISORROPIA II. It was found that particulate liquid water was more sensitive to nitrate than sulfate, and played significant roles in the heterogeneous aqueous reactions of NO_2 and secondary nitrate formation during haze episodes, especially in the high-sulfate haze episode. Further analysis indicated that the high-nitrate haze episode favoured the occurrence of heterogeneous aqueous phase oxidation of SO_2, and the more water was in the particles, the more SO_2 was converted to sulfate aerosols. This work provides an important field measurement-based evidence for understanding the important contributions of the heterogeneous aqueous reactions to secondary aerosol pollution and the tendencies of heterogeneous aqueous reactions in the formation of secondary sulfate and nitrate aerosols in suburban Shanghai.

* Corresponding authors.
E-mail addresses: ldkong@fudan.edu.cn, (L. Kong), jmchen@fudan.edu.cn. (J. Chen).

https://doi.org/10.1016/j.scitotenv.2018.04.086
0048-9697/

1. Introduction

In recent years in China, rapid urbanization and industrialization have resulted in serious air pollution in many cities and regions (Huang et al., 2014; Wang et al., 2015; Zheng et al., 2015), and haze episodes have occurred frequently. One of the severest events is the winter haze which occurred in January 2013 in China (Zheng et al., 2015), with a maximum $PM_{2.5}$ hourly concentration of 772 μg m^{-3} (Huang et al., 2014). This extremely severe and persistent haze episode covered a land area of approximately 1.4 million km^2 and influenced about 800 million people (Cheng et al., 2014). In the winter of 2016, China faced the similarly severe particulate matter (PM) pollution again across vast areas (Yin and Wang, 2017). Haze episodes affect air quality, visibility, human health and climate. Therefore, haze has been investigated extensively (Fu and Chen, 2017). Up to now, many short-term, continuous or persistent haze episodes have been extensively studied (Du et al., 2011; Guo et al., 2014; Hua et al., 2015; Li et al., 2017; Yang et al., 2015; Zheng et al., 2015). High pollutant emissions, adverse meteorological conditions and elevated PM concentrations are largely responsible for the haze formation in many regions (Cheng et al., 2014; Huang et al., 2014), and the occurrence of haze episodes is also closely related to the number concentration, size distribution, chemical composition and mixing state of aerosol particles (Wang et al., 2009; Whiteaker et al., 2002). In China, haze is defined as a weather phenomenon in which the horizontal visibility is <10 km and the relative humidity (RH) is below 80% (QX_T113, 2010). Visibility degradation due to PM is generally related to scattering by sulfate, nitrate, ammonium, and certain organic carbon (OC) as well as absorption by elemental carbon (EC) and some other OC (Andreae et al., 2008; Laskin et al., 2010; Sun et al., 2006). Changes in the chemical composition and the mixing state of particles further complicate their impacts on visibility. Acquiring of highly time-resolved variations in atmospheric aerosol ionic composition and concentration on haze days would provide more information for deep understanding of the variability in atmospheric aerosol chemistry and the characteristics of haze formation.

Previous studies suggested that the reduction of solar radiation intensities in haze episodes weakened atmospheric photochemistry and thereby reduced oxidant concentrations (*e.g.* OH radical), which made gas-phase production of sulfate and nitrate unlikely to be important (Liu et al., 2016; Quan et al., 2015; Zheng et al., 2015). However, the enhanced formation of secondary inorganic aerosol (SIA: NO_3^-, SO_4^{2-} and NH_4^+) in haze episodes has been demonstrated by many previous studies (Qiao et al., 2015; Hua et al., 2015), and therefore the enhanced formation of SIA is usually attributed to heterogeneous reactions. The elevated SIA on haze days not only increases $PM_{2.5}$ concentration, but also increases the hygroscopicity of aerosol particles, and in turn promotes the aqueous-phase reactions for secondary aerosol formation (Qiao et al., 2015; Qiao et al., 2016), resulting in pollution intensification (Han et al., 2016; Liu et al., 2016; Wang et al., 2012; Zheng et al., 2015). Nowadays, heterogeneous aqueous reactions are often used to explain the enhanced production of secondary sulfate and nitrate aerosols during haze (Ma et al., 2017; Quan et al., 2015; Wang et al., 2012). However, the details about the roles of heterogeneous aqueous reaction in the formation of SIA and the occurrence of haze remain poorly understood.

Baoshan District, as a typical suburb of Shanghai, located at the intersection of the Yangtze River and the Huangpu River, is the seaway gate of Shanghai with a total area of 425 km^2 and a population of 1.22 million. It is connected to over 400 harbors in the world with a developed multi-modal transportation and inland navigation network. As a world level industry concentration and expansion area for refined steel manufacturing and relevant industries, Baoshan district owns a large number of large-sized enterprises at state or city level, including BaoSteel, which is the biggest steel producer in China. However, the rapid development of Baoshan district is accompanied by its declining air quality. Haze episodes caused by atmospheric PM have occurred frequently in Baoshan district, particularly in winter. The rapid increases of vehicles and coal consumption in Baoshan district have been regarded as the main reasons for the deterioration of air quality. SO_2, NO_x, TSP, PM_{10}, $PM_{2.5}$, CO, VOC and NH_3 are the main pollutants discharged by the steel manufacturing and relevant industries, of which the emissions of SO_2, NO_x, TSP, CO are significantly higher than other pollutants (Wang et al., 2013). However, to our knowledge, there have been few specific studies focused on high temporal resolution observations conducted to characterize $PM_{2.5}$ and its composition during haze episodes occurring in Baoshan district, which is preventing a comprehensive understanding of the air pollution status in Shanghai. Besides, study on water-soluble ions in $PM_{2.5}$ at high time resolution during haze days is helpful for acquiring more details about haze. Thus, the main objective of this study is to get a deeper understanding of the characteristics of SIA and haze formation, and to elucidate the trends in heterogeneous aqueous reaction in continuous haze episodes in Baoshan district based on high time resolution online water-soluble ions in $PM_{2.5}$.

2. Experiment and methods

2.1. Site description and sampling time

The sampling site of MARGA (31°23′N, 121°26′E) was located on the roof of environmental monitoring station in Baoshan district, which is a typical suburb located at the convergence point of the Huangpu River and the Yangtze River, in the northern part of Shanghai. The geographic distribution of the field experiment site in this study is shown in Fig. 1.

This site is representative of metropolitan industrial zone due to the mixed influence of residential, land traffic, harbor and industrial emissions. The online sampling time was from February 1 to April 29, 2011, and in the study the continuous haze episodes, which occurred from February 18 to February 28, 2011, were selected as studied cases.

2.2. Experiment instruments

Hourly mass concentrations of major water-soluble inorganic ions (NH_4^+, Na^+, K^+, Ca^{2+}, Mg^{2+}, SO_4^{2-}, NO_3^- and Cl^-) were continuously measured using an on-line analyzer (MARGA, model ADI 2080, Applikon Analytical B. V. Corp., Netherlands) with a $PM_{2.5}$ sharp-cut cyclone inlet. Details of the instrument have been described preciously (Du et al., 2011; Kong et al., 2014). Briefly, the system consists of a sampling box and an analytical box. The sampling box is comprised of one wet rotating denuder (WRD) for gas sampling and one steam jet aerosol collector (SJAC) for aerosol collecting. Ambient air was drawn into the sampling box at a flow rate of 1 m^3/h through the inlet by a pump equipped with a mass flow controller, and gaseous components were scavenged and dissolved in the liquid film formed by the WRD, then aerosol species were continuously collected by the SJAC where condensation of steam made aerosols become aqueous droplets rapidly. Subsequently, the two collected liquid samples were analyzed by ion chromatography (IC, conductivity detector, C4 100 × 4 mm column and 3.20 mM HNO_3 eluent for cation, A Supp 10–75 column and 7.00 mM Na_2CO_3 + 8.00 mM $NaHCO_3$ eluent for anion). MARGA was continuously controlled by an internal calibration method using bromide for the anion chromatograph and lithium for the cation chromatograph at 1-h time resolution. MARGA was also calibrated by using external standard solution (mixed cation and anion standards, Dionex Company) in a routine time to ensure the accuracy of data.

2.3. Atmospheric and meteorological data

In this study, the hourly atmospheric parameters including mass concentrations of SO_2, NO_x, O_3 and $PM_{2.5}$ and meteorological parameters including temperature (T), relative humidity (RH), wind speed (WS), visibility (Vis) *etc.* were obtained from local meteorological site, which is located at a distance of 180 m from the sampling site.

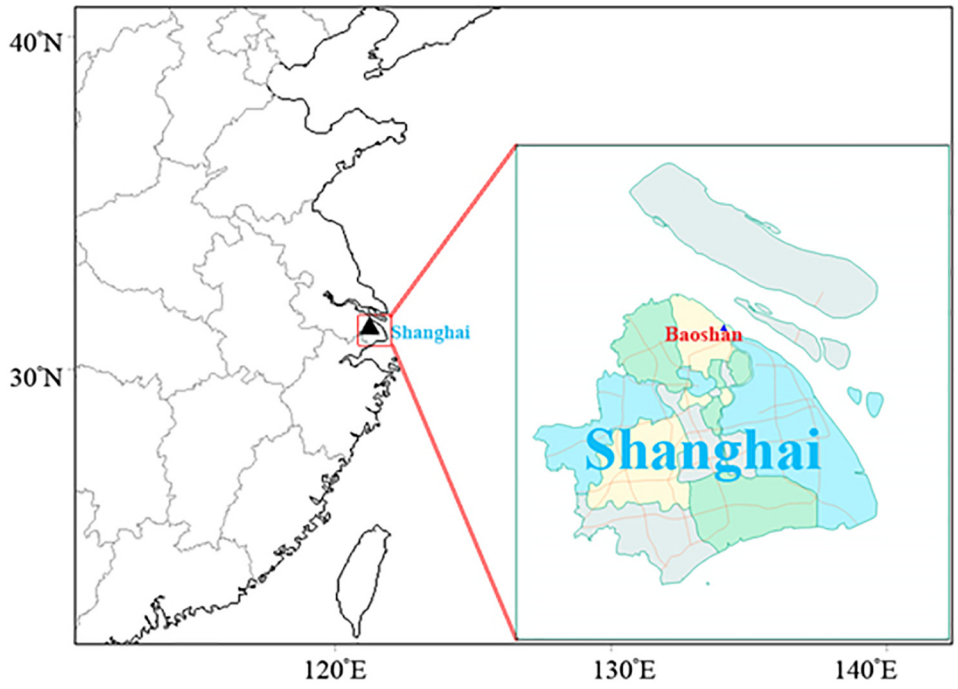

Fig. 1. Map of the geographical location of the sampling site.

2.4. Back trajectory analysis

48-h backward trajectories of air masses arriving at the sampling site were calculated using the HYSPLIT model (http://ready.arl.noaa.gov/HYSPLIT.php) to investigate the influence of different air masses from distant sources on aerosol composition. The meteorological data fields used to run the model are available at NOAA's ARL archives.

2.5. Thermodynamic model

Both free H^+ concentration ($[H^+]_{Ins}$, the square brackets indicate the molar concentration of the species inside, used here and henceforth) and *in situ* pH in the deliquesced particles were used as indicators of aerosol acidity. In this study, in order to explore the characteristics of acidity of $PM_{2.5}$ on haze days, we employed the available and widely used aerosol inorganic model E-AIM (Aerosol Inorganic Model: E-AIM, http://www.aim.env.uea.ac.uk/aim/aim.php) (Clegg et al., 1998; Friese and Ebel, 2010). The E-AIM can be used to simulate gas/aerosol partitioning processes and calculate the equilibrium composition of the aqueous phase or solid aerosol phase. E-AIM 4 is a state-of-the-art model that can accurately simulate the aqueous phase and solid phase of ionic compositions in the mixing system H^+-NH_4^+ -SO_4^{2-} -NO_3^--Cl^--Na^+–H_2O at a given temperature and RH (Clegg et al., 1998). The hourly averaged T, RH, SO_4^{2-}, NO_3^-, Cl^-, NH_4^+, Na^+ and molar concentrations of total aerosol acidity ($[H^+]_{Total}$) were used as the input in model *E*-AIM 4 to obtain the concentrations of free ions (*e.g.* H^+, HSO_4^-) in the aqueous phase and any salt of these ions that was formed in the solid phase at equilibrium. The mole fraction and activity coefficient of each ion in aqueous phase as well as particulate liquid water content were also reported. The $[H^+]_{Total}$ was estimated from the ionic balance of the relevant ionic species (Kong et al., 2014; Pathak et al., 2009; Zhang et al., 2007):

$$[H^+]_{Total} = 2 \times \left[SO_4^{2-}\right] + [NO_3^-] + [Cl^-] - [NH_4^+] - [Na^+] \quad (1)$$

Based on the model outputs, the *in situ* particle pH was calculated as follow:

$$\textit{in situ} \text{ particle pH} = -\lg\left(\gamma \times [H^+]_{Frac}\right) \quad (2)$$

where γ and $[H^+]_{Frac}$ are the activity coefficient on mole fraction basis and the molar fraction of aqueous phase H^+, respectively. While $\gamma \times [H^+]_{Frac}$ represents the aqueous phase activity of H^+ (Zhang et al., 2007).

For comparison, ISORROPIA II thermodynamic equilibrium model (available at http://isorropia.eas.gatech.edu) was employed to compute the equilibrium composition in the aerosol system Na^+ - K^+ - Ca^{2+} - Mg^{2+} - NH_4^+ - SO_4^{2-} - NO_3^- - Cl^- - H_2O (Fountoukis and Nenes, 2007; Nenes et al., 1998). The forward mode in ISORROPIA II was used, and the model was run by assuming that aerosol solutions were metastable (only a liquid phase) (Bougiatioti et al., 2016; Guo et al., 2016). Input to the model included the total gas + aerosol concentrations of SO_4^{2-}, $HNO_3 + NO_3^-$, $HCl + Cl^-$, $NH_3 + NH_4^+$, Na^+, K^+, Mg^{2+} and Ca^{2+}, along with simultaneously measured T and RH. The particle pH was calculated using the following equation (Liu et al., 2017):

$$\text{particle pH} = -\lg\left(1000[H^+]_{ISO}/[H_2O]_{ISO}\right) \quad (3)$$

where $[H^+]_{ISO}$ ($\mu g/m^3$) is the equilibrium particle hydronium ion concentration per volume air, and $[H_2O]_{ISO}$ ($\mu g/m^3$) is the particulate liquid water content output from ISORROPIA II.

3. Results and discussion

3.1. General characteristics of haze episodes

The experiments were performed using MARGA to continuously monitor mass concentrations of major water-soluble inorganic ions in $PM_{2.5}$ at 1-h time resolution. The time series of hourly mass concentrations of $PM_{2.5}$, total water-soluble ions (TWSI), SIA and other water-soluble ions during observation period from February 18 to February 28 are shown in Fig. 2, and the meteorological and chemical data on haze and non-haze days are summarized in Table 1. The shaded parts

in gray in Fig. 2 indicate the haze episodes reported by Baoshan meteorological station. Three reported haze episodes occurred on February 18 (denoted as Haze I), 21 (denoted as Haze II) and 27 (denoted as Haze III) during the 10-day observation period in winter, showing the high occurrence of haze episodes in Baoshan district during this period.

3.1.1. Characteristics of $PM_{2.5}$ concentrations during haze episodes

Fine particle pollution in Baoshan was serious during the observation period. The average concentration of $PM_{2.5}$ was 54.5 μg/m^3 during the whole sampling period, which exceeded the first grade of the Chinese National Ambient Air Quality Standard for daily averaged $PM_{2.5}$ concentration (CNAAQS, GB3095–2012, 35 μg/m^3) and the 24-h limit of the US National Ambient Air Quality Standard for $PM_{2.5}$ (35 μg/m^3, USEPA, 1997). As shown in Fig. 2a, the $PM_{2.5}$ concentrations of three haze days were higher than that of non-haze days, and the highest concentration of $PM_{2.5}$ even reached to 199 μg/m^3 on Feb. 21. During the sampling period, the average mass concentrations of $PM_{2.5}$ were 79.4 μg/m^3 and 42.6 μg/m^3 on haze days and non-haze days, respectively, and the value of haze days was 1.86 times higher than that of non-haze days. These results indicated that $PM_{2.5}$ was closely associated with the occurrence of haze, and high $PM_{2.5}$ mass concentrations often resulted in low visibility. The average mass concentration of $PM_{2.5}$ on haze days was slightly higher than the second grade of the Chinese ambient air quality standard (GB3095-2012, 75 μg m^{-3} for $PM_{2.5}$ for second grade), indicating that atmospheric fine particle pollution in Baoshan district during haze episodes was serious. In addition, it is noteworthy that high mass concentrations of $PM_{2.5}$ shown in Fig. 2a are not always in one-to-one correspondence with the occurrence of haze, indicating that some other factors should exist to influence the occurrence of haze, such as the formation of secondary aerosols, meteorological conditions and weather systems.

3.1.2. Characteristics of water-soluble ions in $PM_{2.5}$ during haze episodes

Chemical composition of atmospheric $PM_{2.5}$ is very complex, which includes sulfate, nitrate, ammonium, organic carbon, inorganic carbon and metal elements, among which water-soluble inorganic ions are one of the most important components. In this study, the average mass concentrations of TWSI and SIA were 47.2 and 42.9 μg/m^3 on haze days and 20.6 and 18.6 μg/m^3 on non-haze days, respectively (Table 1). TWSI accounted for 59.4% of the $PM_{2.5}$, and SIA accounted for 54.1% of $PM_{2.5}$ and 91.0% of the TWSI during the haze periods, respectively. While during the non-haze periods, TWSI accounted for 48.4% of the $PM_{2.5}$, and SIA accounted for 43.5% of $PM_{2.5}$ and 90.0% of the TWSI, respectively. Obviously, the TWSI and SIA on haze days contributed more to the mass concentrations of $PM_{2.5}$ than those on non-haze days.

As shown in Fig. 2a, the mass concentrations of TWSI and SIA were quite close through the entire period, and their trends matched perfectly with $PM_{2.5}$. The TWSI and SIA on haze days had a good positive correlation with $PM_{2.5}$, respectively, and the linear correlation coefficient (r) of TWSI and SIA with $PM_{2.5}$ were 0.78 and 0.77, respectively. Fig. 2a also shows that during the haze days not only the hourly average mass concentrations of $PM_{2.5}$ significantly increased, but also those of TWSI and SIA had obvious increases than usual, which demonstrated the enhanced formation of SIA in haze episodes. This result is consistent with the previous studies (Zhao et al., 2015a, 2015b; Park and Kim, 2004; Wang et al., 2016a; Wang et al.,2016b). Moreover, as shown in Fig. 2a, haze episodes were accompanied by a breakthrough of 75.0 μg/m^3 in the hourly mass concentration of SIA, indicating that the enhanced formation of SIA played an important role in triggering the occurrence and evolution of haze episodes (Liu et al., 2016). In addition, high SIA levels on haze days facilitated the hygroscopic growth of aerosols due to a good positive correlation between SIA and particulate liquid water ($r = 0.89$) (Table 1), which in turn promoted the aqueous-phase reactions for SIA formation (Qiao et al., 2016). Hygroscopic secondary sulfate and nitrate aerosols also have a potential influence on water-soluble SOC formation, though the water-soluble SOC has not been measured in our study (Xiang et al., 2017). Therefore, the high concentrations of TWSI and SIA would lead to high concentration of $PM_{2.5}$ on haze days.

The average mass concentrations of SO_4^{2-}, NO_3^-, and NH_4^+ were 16.1, 15.3 and 11.2 μg/m^3 on haze days, respectively, while 6.9, 5.9 and 4.4 μg/m^3 on non-haze days, respectively. The average mass concentrations of SO_4^{2-}, NO_3^- and NH_4^+ on haze days were 2.33, 2.58 and 2.53 times higher than those on non-haze days, respectively, indicating that SO_2 and NO_2 were more inclined to transform into secondary

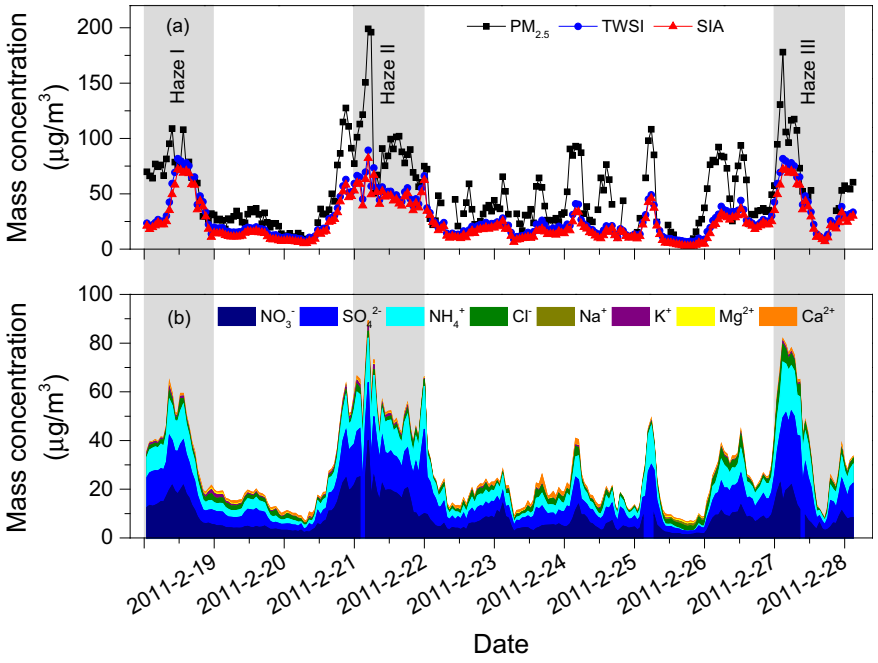

Fig. 2. Time series of hourly mass concentrations of $PM_{2.5}$, TWSI, SIA and other water-soluble inorganic ions from February 18 to February 28. The shaded areas in gray represent the identified haze periods.

Table 1
Summary of meteorological and chemical data on haze and non-haze days.

Parameters/species	Haze I	Haze II	Haze III	Average	Non-haze days
$PM_{2.5}$ (μg/m^3)	67.4 ± 22.3	99.4 ± 37.0	67.9 ± 42.4	79.4 ± 36.7	42.6 ± 25.0
O_3 (μg/m^3)	45.9 ± 8.9	62.3 ± 20.0	19.6 ± 6.2	42.6 ± 21.9	32.6 ± 13.0
SO_2 (μg/m^3)	28.5 ± 8.1	28.8 ± 11.7	60.3 ± 34.2	39.2 ± 25.9	29.5 ± 16.7
NO_2 (μg/m^3)	28.4 ± 6.9	38.2 ± 19.4	58.3 ± 17.2	41.6 ± 19.7	50.2 ± 29.4
NO_x (μg/m^3)	31.2 ± 9.6	40.3 ± 21.6	108.8 ± 58.0	60.1 ± 49.9	83.4 ± 77.6
SO_4^{2-} (μg/m^3)	13.1 ± 4.7	17.6 ± 3.3	17.4 ± 10.0	16.1 ± 6.9	6.9 ± 5.2
NO_3^- (μg/m^3)	13.8 ± 5.1	20.5 ± 5.5	11.7 ± 5.8	15.3 ± 6.6	5.9 ± 3.6
NH_4^+ (μg/m^3)	9.4 ± 3.5	12.7 ± 2.9	11.4 ± 6.2	11.2 ± 4.6	4.4 ± 3.2
SIA (μg/m^3)	36.4 ± 13.3	49.5 ± 10.3	44.1 ± 22.3	42.9 ± 16.1	18.6 ± 10.3
TWSI (μg/m^3)	40.5 ± 13.5	54.8 ± 11.3	46.2 ± 23.5	47.2 ± 17.5	20.6 ± 11.1
SIA/TWSI	0.88 ± 0.06	0.91 ± 0.02	0.88 ± 0.03	0.89 ± 0.05	0.80 ± 0.09
SIA/$PM_{2.5}$	0.54 ± 0.07	0.49 ± 0.11	0.58 ± 0.08	0.53 ± 0.09	0.42 ± 0.13
NO_3^-/SO_4^{2-}(mass ratio)	1.05 ± 0.40	1.18 ± 0.20	0.78 ± 0.28	1.00 ± 0.26	0.99 ± 0.37
SOR	0.23 ± 0.03	0.31 ± 0.09	0.18 ± 0.10	0.24 ± 0.09	0.14 ± 0.09
NOR	0.26 ± 0.07	0.30 ± 0.09	0.13 ± 0.04	0.23 ± 0.10	0.09 ± 0.06
$[H^+]_{Total}$ (nmol/m^3)	34.1 ± 24.4	98.7 ± 63.6	63.1 ± 42.0	62.0 ± 51.4	55.5 ± 32.6
$[HSO_4^-]$ (nmol/m^3)	21.2 ± 15.6	54.5 ± 27.7	41.1 ± 26.7	35.8 ± 26.3	25.6 ± 15.0
$[H^+]_{ins}$ (nmol/m^3)	12.3 ± 11.9	44.4 ± 34.8	22.0 ± 17.7	23.3 ± 24.5	33.4 ± 45.3
Particulate liquid water (μg/m^3)	45.2 ± 35.7	107.0 ± 79.4	55.7 ± 24.8	63.7 ± 53.1	36.7 ± 29.9
In situ aerosol pH	2.39 ± 0.83	2.34 ± 0.46	2.34 ± 0.55	2.36 ± 0.65	1.83 ± 0.74
T (°C)	3.7 ± 1.4	6.0 ± 3.3	12.3 ± 2.4	7.3 ± 4.4	8.3 ± 3.2
RH (%)	73.7 ± 8.4	73.7 ± 15.8	76.9 ± 3.9	74.8 ± 10.5	74.0 ± 12.6
Wind speed (m/s)	2.3 ± 1.0	2.3 ± 1.2	2.9 ± 1.5	2.5 ± 1.3	2.9 ± 1.5
Visibility (km)	4.9 ± 2.2	3.3 ± 1.9	4.9 ± 2.3	4.4 ± 2.3	12.5 ± 9.6

particles during haze days and thus further increased atmospheric fine particle pollution. The trends for the average concentrations of SIA in $PM_{2.5}$ in the three haze episodes were as follows: NO_3^- > SO_4^{2-} > NH_4^+ for Haze I and Haze II, and SO_4^{2-} > NO_3^- > NH_4^+ for Haze III (see Fig. 2b and Table 1), showing the differences in SIA formation in different haze episodes. In Haze I and Haze II, NO_3^- exceeded SO_4^{2-} and became the most abundant inorganic ionic species of $PM_{2.5}$, whereas in Haze III SO_4^{2-} was still the most abundant inorganic ionic species of $PM_{2.5}$. Therefore, in this study Haze I and Haze II are seen as high-nitrate haze episodes, while Haze III is seen as a high-sulfate haze episode. High occurrence of high-nitrate haze episodes indicated that nitrate pollution presented increasing trend, which should be attributed to SO_2 reduction and increase in NO_x emission due to SO_2 emission control strategies of China as well as the rapid increase of NO_x emitted from dramatically increased vehicle population.

The average concentrations of Ca^{2+} and Mg^{2+} were 0.9 and 0.2 μg/m^3 on haze days, respectively, whereas 0.9 and 0.3 μg/m^3 on non-haze days, respectively. The average concentrations of Ca^{2+} in Haze I, II and III were 0.8, 1.1 and 0.9 μg/m^3, respectively. The concentrations of Ca^{2+} and Mg^{2+} did not vary much on haze and non-haze days and could be reasonably attributed to soil dust rather than dust storm. Low concentrations of Na^+ in $PM_{2.5}$ on haze days suggested low contribution of marine aerosol source, even if air masses crossed the marine areas (Fig. 3a, b), and therefore low marine source contributing to Cl^-. The 48 h -back trajectories at 500 m and 1000 m showed that the air mass of Haze I episode came from northeastern China (Fig. 3a), where high pollutant emissions had been observed due to the coal combustion as well as the industrial discharge. While the air mass of Haze II episode came from the Korean Peninsula, and crossed the Yellow Sea where ship emission was concerned (Fig. 3b). Therefore, the formation of Haze I and Haze II should be associated with the long-range transport of air pollutants and local secondary pollution. The analysis of 48 h -back trajectory also indicated that there was no influence of direct marine air masses in the Haze III (Fig. 3c), and it occurred on Feb 27 was a complicated pollution episode concerning intra-regional transport. During the Haze III, the air masses at 500 m and 1000 m were mainly transported from Jiangsu, Anhui and Zhejiang provinces in the Yangtze River Delta region where also suffered from heavy pollution, which brought some polluted air into the transported air parcels and affected the ground-level air quality at the sampling site during this period, resulting in the higher average mass concentration of SIA. K^+ is often used as an indicator for estimating biomass burning emission and tracing long-range transport of carbonaceous aerosol in the atmosphere (Ding et al., 2017; Yao et al., 2016). In our study, the average concentration of K^+ on haze days was 0.9 μg/m^3, and the average concentrations of K^+ in Haze I, II and III were 1.0, 1.3 and 0.5 μg/m^3, respectively. These values were lower than the 3-year average of K^+ mass concentration in February that was observed in urban Shanghai from 2011 to 2013 (3.0 μg/m^3) (Wang et al., 2016a; Wang et al.,2016b), indicating that the biomass burning emission was as usual and no large-scale biomass burning appeared during the sampling period. Cl^- in $PM_{2.5}$ is usually thought to be from sea salt, fossil fuel combustion and biomass burning. In our study, low marine source contribution and no correlation between Cl^- and K^+ ($r^2 = 0.01$) during the haze days indicated that measured Cl^- in $PM_{2.5}$ was mainly from fossil fuel combustion. Therefore, the 3 haze episodes occurred on Feb 18, 21 and 27 were mainly influenced by secondary aerosol pollution, while secondary pollution could be ascribed to local pollution and regional transport impact.

In addition, the mass ratio of $[NO_3^-]/[SO_4^{2-}]$ has been used as an indicator of the relative importance of stationary *vs.* mobile sources of sulfur and nitrogen in the atmosphere (Arimoto et al., 1996; Yao et al., 2002). High $[NO_3^-]/[SO_4^{2-}]$ mass ratio means the predominance of mobile source over stationary source of pollutants (Arimoto et al., 1996), and *vice versa*. During the observation period from February 18 to February 28, the average mass ratio of $[NO_3^-]/[SO_4^{2-}]$ was 0.996. The average mass ratios of $[NO_3^-]/[SO_4^{2-}]$ on haze days and non-haze days were 1.00 and 0.99, respectively. Compared to the previous studies, the $[NO_3^-]/[SO_4^{2-}]$ mass ratio of our observation was higher than those of Shanghai urban in 1999–2000 (0.43) (Yao et al., 2002), 2009 (0.67) (Zhao et al., 2015a, 2015b), and 2012 (0.86) (Zhao et al., 2015a, 2015b). The $[NO_3^-]/[SO_4^{2-}]$ mass ratio of our study was also higher than those of most European cities where average mass ratio was 0.84 (Putaud et al., 2004). The results indicated that mobile source such as vehicles gradually became more and more dominant, which is consistent with high occurrence of high-nitrate haze episodes. Baoshan district owns a large number of large-sized industries covering iron and steel, storage and transport, energy, and water resources. The fossil fuel burning mills such as Baosteel and Shidongkou Power Plant discharge large quantities of sulfur dioxide to the atmosphere. Besides, Baoshan district has well-developed seafaring and land transport as it is an important industrial production and exportation base that would discharge large

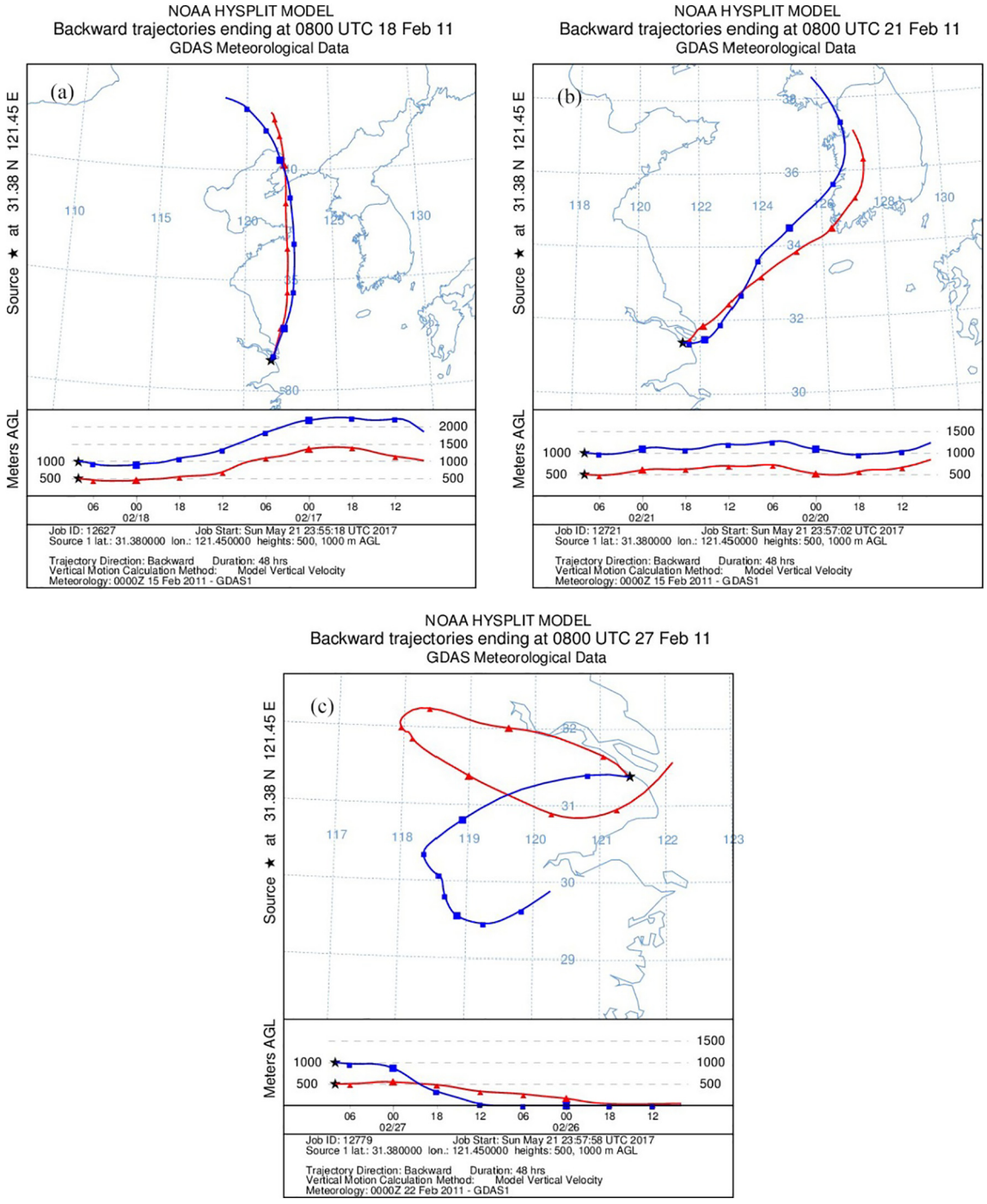

Fig. 3. 48-h Back trajectories on the selected haze days: (a) Haze I, (b) Haze II and (c) Haze III.

quantities of nitrogen oxides to the atmosphere. The high mass ratio of $[NO_3^-]/[SO_4^{2-}]$ and high mass concentrations of SO_4^{2-} and NO_3^- during our observation period indicated that both stationary and mobile sources were heavy emitters. These results clearly showed Baoshan district had its own unique characteristics of air pollution.

3.1.3. Characteristics of gaseous pollutants and meteorological parameters on haze days

Secondary sulfate and nitrate aerosols in the atmosphere are originated primarily from the conversions of gaseous precursors such as SO_2 and NO_x. These precursors released by anthropogenic sources are the main contributors to secondary aerosols. Fig. 4 presents an overview of the temporal variations in the concentrations of $PM_{2.5}$, SIA, SO_4^{2-}, NO_3^- and main gas-phase species such as SO_2, NO_2 and O_3, as well as meteorological and other chemical parameters during the study period from February 18 to February 28. As shown in Fig. 4, overall average mass concentrations of SO_2 and NO_2 in Haze I were close to each other, while overall average mass concentration of SO_2 was lower than that of NO_2 in Haze II, and in terms of Haze III, overall average mass concentration of SO_2 was higher than that of NO_2. The average mass concentrations of SO_2 in Haze I, Haze II and Haze III were 28.5, 28.8 and 60.3 μg/m^3, respectively. SO_2 concentration in Haze III was much higher than that in Haze I and Haze II. The average mass concentrations of NO_2 in Haze I, Haze II and Haze III were 28.4, 38.2 and 58.3 μg/

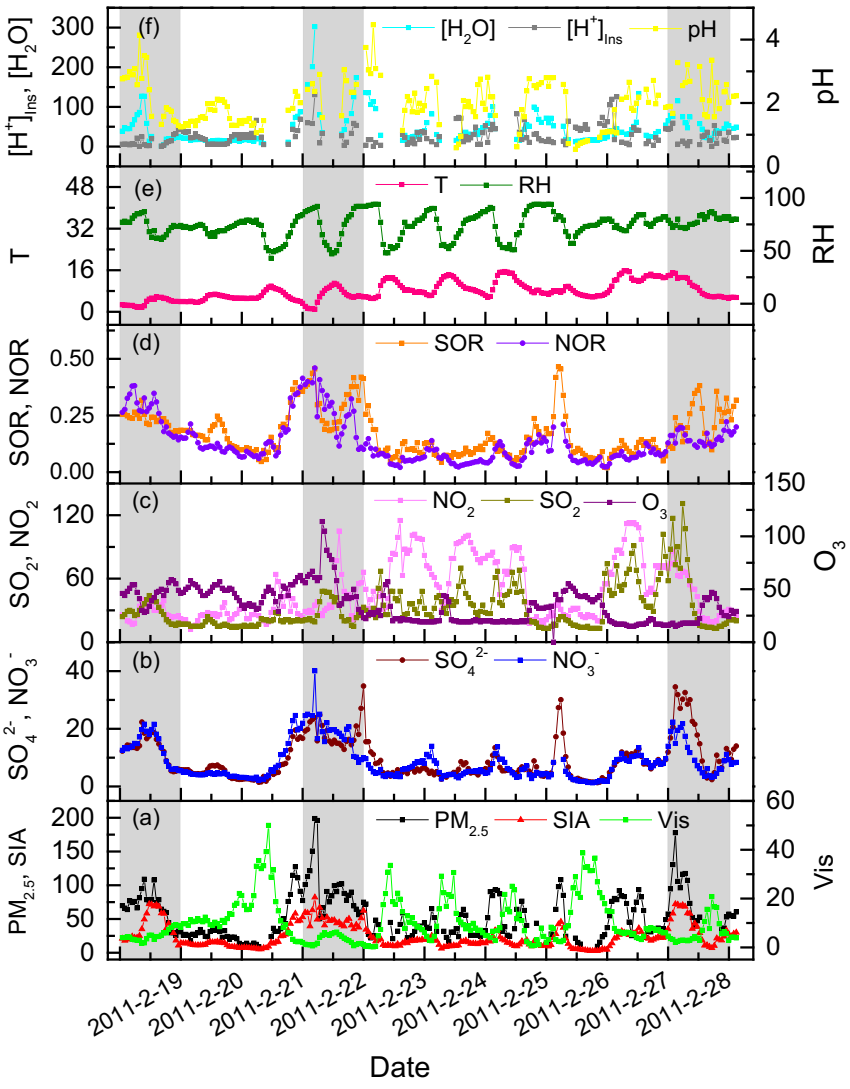

Fig. 4. Time series of selected parameters from February 18 to February 28. (a) $PM_{2.5}$ (μg/m^3), SIA (μg/m^3) and visibility (Vis, km); (b) SO_4^{2-} and NO_3^- (μg/m^3); (c) SO_2, NO_2 and O_3(μg/m^3); (d) Sulfur oxidation ratio (SOR) and nitrogen oxidation ratio (NOR); (e) temperature (T, °C) and relative humidity (RH, %); (f) particulate water ([H_2O], μg/m^3), $[H^+]_{Ins}$ (nmol/m^3) and pH. The shaded areas in gray represent haze periods.

m^3, respectively. The average mass concentrations of SO_2 and NO_2 were 39.2 and 41.6 μg/m^3 on haze days, respectively, whereas 29.5 and 50.2 μg/m^3 on non-haze days, respectively (Table 1).

Stable meteorological factors play a vital role in the formation of haze episodes. Generally, low mixed layer height (MLH) and weak wind speed on haze days can decrease atmospheric dispersion capacity, result in the accumulation of atmospheric pollutants, and thus enhance PM and gas pollutant concentrations. In our study, it is found that the concentrations of SO_2, NO_2 and NO_x in Haze I and II were lower than those on non-haze days, respectively. One of the reasons for this phenomenon may be due to the similar average mixed layer height and the similar average wind speed on haze days (400 m, 2.5 m/s) and non-haze days (374 m, 2.9 m/s) (Table 1, Fig. S1). This result may also imply high emissions of SO_2 and NO_x due to tremendous consumption of fossil fuel from industry and vehicles in Baoshan district, even on non-haze days. The average mass concentrations of O_3 in Haze I, Haze II and Haze III were 45.9, 62.3 and 19.6 μg/m^3, respectively, whereas the average solar radiation (SR) intensities in Haze I, Haze II and Haze III were 142, 231 and 132 W/m^2, respectively. Meanwhile, as shown in Fig. 4c, the increase of O_3 concentrations in the afternoon in Haze I, II and III and the formation of O_3 in the morning in Haze I and II were observed. These may imply the photochemical formation of O_3 to different extents, though low SR on haze days rendered high photochemical activity impossible. Significant reductions of O_3 mass concentrations were observed due to the dimming effect of high loading of aerosol particles or secondary aerosols (Fig. 4a–c) (Zheng et al., 2015). Moreover, the lower O_3 concentration in Haze III might be attributed to the high concentrations of SO_2 and NO (NO═NOx-NO_2, 50.5 μg/m^3, see Table 1) in the morning, as well as weak contribution of photochemical formation in the afternoon due to low SR (Fig. S1). These results showed diverse characteristics of gas-phase species and meteorological conditions on different haze days in Baoshan district.

3.2. $PM_{2.5}$ acidity in haze episodes

3.2.1. Comparison of particle pH values predicted by E-AIM 4 and ISORROPIA II

In this study, particle pH is calculated using the latest E-AIM 4 and ISORROPIA II thermodynamic models. E-AIM is usually considered as an accurate benchmark model (Seinfeld and Pandis, 2016), and it can be used to evaluate the performance of ISORROPIA II (Liu et al., 2017). This model has been used by many previous studies (*e.g.* Hodas et al., 2014; Hoyle et al., 2016; Parworth et al., 2017). As for ISORROPIA, it employs a number of simplifications to make it computationally efficient for application in large-scale atmospheric models (Fountoukis and Nenes, 2007). For example, activity coefficient of hydrogen ions is

assumed to be equal to unity (Fountoukis and Nenes, 2007). ISORROPIA II treats more crustal ionic species (*i.e.*, Ca^{2+}, K^+, and Mg^{2+}) compared to *E*-AIM 4. These may lead to the deviation in pH predicted by the forward modes of E-AIM 4 and ISORROPIA II.

We compared the calculated particle pH from ISORROPIA with those from E-AIM 4 (Fig. S2). From E-AIM 4 calculation, the average particle pH during the whole study period was 1.97, and the average particle pH on haze days and non-haze days were 2.36 and 1.83 (Table 1), respectively. While from the ISORROPIA II calculation, the average particle pH during the whole study period was 3.07, and the average particle pH on haze days and non-haze days were 2.90 and 3.14, respectively. Obviously, large discrepancies between the particle pH values calculated by *E*-AIM 4 and ISORROPIA II were found on non-haze days and during the whole study period. This likely arose from the differences in treatments of H^+ activity coefficient and crustal ionic species in *E*-AIM 4 and ISORROPIA II calculations, especially relatively high contribution of crustal ionic species (Ca^{2+}, K^+, and Mg^{2+}) to the particle acidity due to the low concentrations of SO_4^{2-} and NO_3^- on non-haze days. However, the average particle pH calculated by E-AIM 4 in Haze I (2.39), II (2.34) and III (2.34) were comparable to those calculated by ISORROPIA II (Haze I: 2.98, Haze II: 2.99 and Haze III: 2.73), respectively, revealing a good agreement between the two models for particle pH calculations on haze days. This result implied a weakening of the contributions of crustal ionic species (Ca^{2+}, K^+, and Mg^{2+}) to the particle acidity due to the high concentrations of SO_4^{2-} and NO_3^- on haze days. This result also demonstrated that the $PM_{2.5}$ particles had strong acidity during the haze episodes whether they were calculated by E-AIM 4 or by ISORROPIA II. Therefore, in view of these results, the discussion concerning particle acidity after this section is mainly based on the results of E-AIM 4 calculation.

3.2.2. In situ aerosol acidity

The $[H^+]_{Ins}$, particulate liquid water ($[H_2O]$) and *in situ* $PM_{2.5}$ pH, which were calculated by E-AIM 4, are shown in Fig. 4. As shown in Fig. 4f, in most cases the *in situ* pH increased with the increasing of particulate liquid water content as the higher water content made the $PM_{2.5}$ less acidic. However, on February 19 the pH increased with the decreasing of RH and $[H_2O]$. This was mainly due to a faster decrease in $[H^+]_{Ins}$ than in RH and $[H_2O]$. The pH had a high negative correlation with $[H^+]_{Ins}$ ($r = -0.65$). Both $[H^+]_{Ins}$ and $[H_2O]$ were the important parameters that determined the *in situ* $PM_{2.5}$ pH.

The average $[H_2O]$, $[H^+]_{Ins}$, $[HSO_4^-]$ and *in situ* $PM_{2.5}$ pH of haze days during the whole sampling period were 63.7 μg/m^3, 23.3 nmol/m^3, 35.8 nmol/m^3 and 2.36, respectively, while these average values on non-haze days during this period were 36.7 μg/m^3, 33.4 nmol/m^3, 25.6 nmol/m^3 and 1.83, respectively (Table 1). The former was less acidic because of its low $[H^+]_{Ins}$ and much higher $[H_2O]$. The $[H^+]_{Ins}$ of haze days was 0.70 times less than that of non-haze days, while the $[H_2O]$ of haze days was 1.73 times more than that of non-haze days. This once again indicated that $[H_2O]$ was one of the most important parameters determining the *in situ* $PM_{2.5}$ pH of the haze episodes during the observation period.

3.3. Particulate liquid water in continuous haze episodes

3.3.1. Characteristics of particulate liquid water on haze days

Liquid water in aerosols provides a surface/interface or a medium for the condensation and/or heterogeneous reaction of atmospheric gaseous species, which would promote the formation of secondary aerosols and their mixing states. It also contributes to visibility degradation. During the whole study period, the particulate liquid water content derived from ISORROPIA II agreed very well with those from *E*-AIM 4 ($r^2 = 0.95$), and their trends matched perfectly with each other (Fig. 5). On haze days, the particulate liquid water calculated from E-AIM 4 had a strong linear correlation with that calculated from ISORROPIA II ($r^2 = 0.97$). Therefore, the following discussion concerning particulate liquid water is still based on the results of E-AIM 4 calculation.

Particulate liquid water is often found to be a combined result of RH and chemical composition (Xue et al., 2014). As shown in Fig. 4, high level of particulate liquid water was often accompanied by high RH and high concentrations of SIA, NO_3^- and SO_4^{2-}, and thus the particulate liquid water had a high linear correlation with RH ($r = 0.71$), SIA ($r = 0.67$), NO_3^- ($r = 0.74$) and SO_4^{2-} ($r = 0.49$). High mass concentrations of SO_4^{2-} shown in Fig. 4 were not always in one-to-one correspondence with high particulate liquid water, which resulted in relatively low correlation coefficient. The linear regression results indicated that particulate liquid water was more sensitive to nitrate than sulfate. In other word, nitrate played a more important role in increasing particulate liquid water content than sulfate, which is consistent with the fact that nitrate has stronger hygroscopic ability to make a particle take up water, especially at high RH (Deng et al., 2016). These results are consistent with the previous reports (Hodas et al., 2014; Xue et al., 2014).

Fig. 6 shows particulate liquid water content and visibility under different RH on haze days and non-haze days. As shown in Fig. 6, a great difference in the variations of particulate liquid water was observed between haze days and non-haze days. On haze days, exponential growth of particulate liquid water was rapid with increasing RH, and the maximum particulate liquid water content was up to 302 μg/m^3 at 91% RH, whereas on non-haze days, exponential growth of particulate liquid water was slow with increasing RH, and the maximum particulate liquid water content was only 80.4 μg/m^3 even at 94% RH. The average mass concentration of particulate liquid water on haze days (63.7 μg/m^3) was higher than that on non-haze days (36.7 μg/m^3) (Table 1). The former should be closely related to high concentrations of secondary nitrate and sulfate due to the similar RH average values on haze days (74.8%) and non-haze days (74.0%). During the high-nitrate haze episodes (Haze I and Haze II), the highest particulate liquid water content (107 μg/m^3) was observed in Haze II, and the level was 1.92 times higher than that in the high-sulfate haze episode (Haze III) despite a similar SO_4^{2-} mass concentration in Haze II and III. One of the reasons for the high particulate liquid water content in Haze II was the presence of high mass concentration of nitrate (Table 1). The increasing particulate liquid water on haze days not only deteriorated visibility in the form of exponential growth as shown in Fig. 6, but also made atmospheric aqueous phase reaction possible.

3.3.2. Heterogeneous aqueous reaction in haze episodes

Many studies have demonstrated the enhanced formation of secondary aerosols in haze episodes, and the enhanced formation of secondary aerosols is often thought to be ascribed to heterogeneous

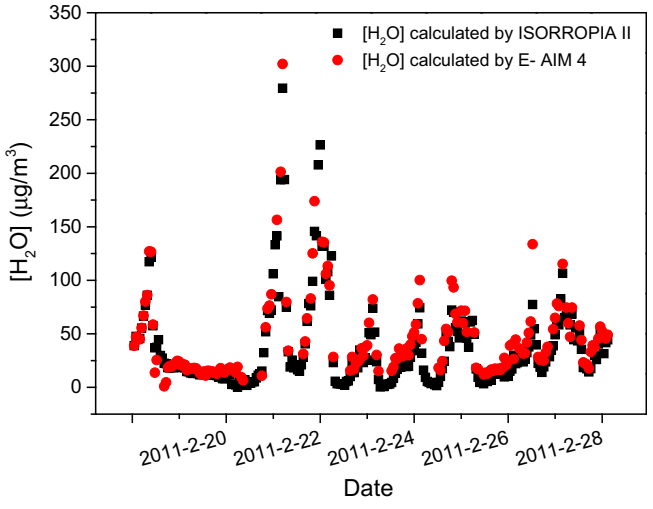

Fig. 5. Relationship between the two $[H_2O]$ values predicted by ISORROPIA II and *E*-AIM 4.

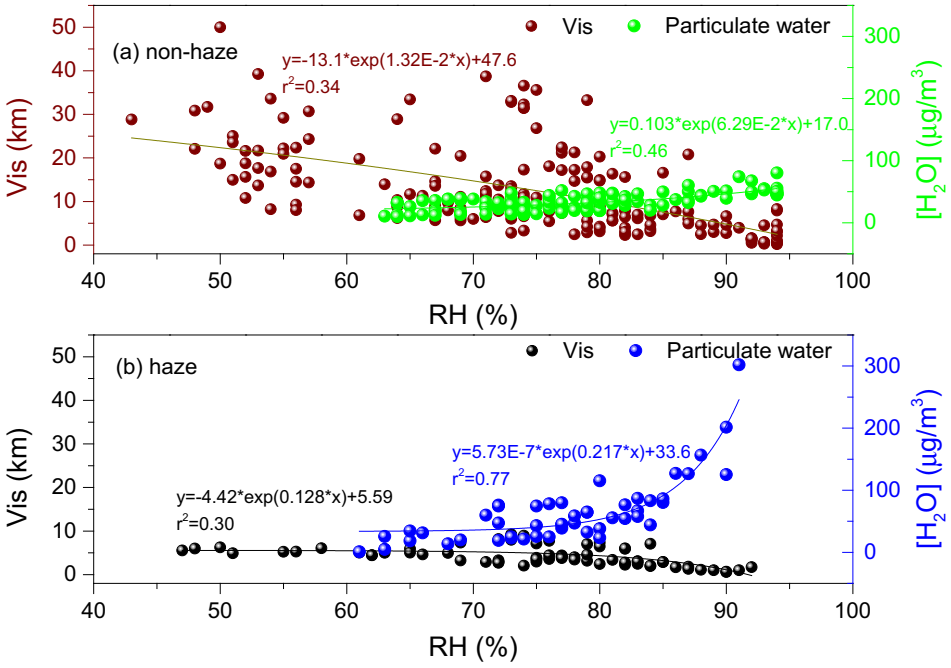

Fig. 6. Particulate liquid water content ([H_2O]) and Visibility (Vis) under different RH on haze days and non-haze days. The lines represent the exponential fits through the data.

aqueous reaction during haze episodes (Hodas et al., 2014; Liu et al., 2016; Qiao et al., 2016; Wang et al., 2012; Xue et al., 2014). Particulate liquid water has an important effect on the occurrence of atmospheric heterogeneous aqueous reactions by providing a reaction medium and accelerating gas-particle transformation of gaseous pollutants, and therefore particulate liquid water plays a significant role in the formation of haze. However, many details about the roles of the particulate liquid water in the atmosphere remain unclear. In this study, high average RH on haze days (74.8%) and non-haze days (74.0%) provided conditions for the occurrence of different heterogeneous aqueous reactions to different degrees.

The chemical formation of sulfate and nitrate could be associated with oxidation rates of SO_2 and NO_2, and therefore sulfur oxidation ratio, defined as SOR = n-NSS-SO_4^{2-}/(n-NSS-SO_4^{2-} + n-SO_2), and nitrogen oxidation ratio, defined as NOR = n-NO_3^-/(n-NO_3^- + n-NO_2), have usually been used as indicators of secondary transformation processes (Sun et al., 2006; Tian et al., 2017). In this study, the average values of SOR and NOR were 0.14 and 0.09 on non-haze days, while 0.24 and 0.23 on haze days, respectively. Correspondingly, the average mass concentrations of SO_4^{2-} and NO_3^- on haze days were 2.33 and 2.58 times higher than that on non-haze days, respectively, indicating the enhanced secondary conversion of SO_2 and NO_2 and the enhanced formation of SIA on haze days.

To understand the roles of heterogeneous aqueous reactions in the formation of secondary sulfate and nitrate aerosols, the relationships of SOR and NOR with particulate liquid water were analyzed. Fig. 7 shows SOR and NOR under different particulate liquid water content on haze days and non-haze days, respectively. As shown in Fig. 7, moderate exponential correlation in Haze I ($r^2 = 0.37$) and strong exponential correlation in Haze II ($r^2 = 0.84$) were found between particulate liquid water and SOR (Fig. 7a), indicating that the SOR presented exponential increase with particulate liquid water in Haze I and II, especially in Haze II. These results suggested that the high-nitrate haze episode favoured the occurrence of heterogeneous aqueous phase oxidation of SO_2, and the more water was in the particles, the more SO_2 was converted to sulfate aerosols. However, no correlation existed between particulate liquid water and SOR in Haze III. Considering the higher average RH (76.9%), the higher levels of SO_2 and NO_x, and the higher concentrations of hygroscopic SO_4^{2-} and NO_3^-, as well as the consistently lower SOR (mostly <0.3 and average value: 0.18) in the Haze III, this result actually presented an evidence for more aqueous-phase oxidation of SO_2. Therefore, this result together with weak photochemistry in Haze III suggested an important contribution of the heterogeneous aqueous reaction to secondary aerosols, and hence the Haze III occurred on Feb 27 was a complicated secondary pollution episode concerning the heterogeneous aqueous reaction processes and intra-regional transport (Park et al., 2016). Fig. 7b shows the exponential increase of NOR with particulate liquid water in the three haze episodes to different degrees, indicating that particulate liquid water played significant roles in the heterogeneous aqueous reactions of NO_2 and the formation of secondary nitrate during haze episodes, especially in the high-sulfate haze episode. While in the high-nitrate haze episodes, the more water was, the more it reflected the effect of heterogeneous aqueous reaction of NO_2 on secondary nitrate formation. In addition, poor correlations between particulate liquid water and SOR or NOR on non-haze days indicated that the heterogeneous aqueous reactions had minor contributions to secondary sulfate and nitrate formation, even at high average RH (74.0%) (Fig. 7c). One possible reason is that the gas-phase oxidation may make a great contribution to the formation of sulfate and nitrate under the conditions of the low loading of $PM_{2.5}$ and the high solar radiation on non-haze days. Another possible reason is that through deliquescence at high RH on non-haze days the low levels of $PM_{2.5}$ cannot provide an adequate amount of reactive aqueous particles that can be comparable with those on haze days, though the formation of sulfate and nitrate aerosols through the heterogeneous aqueous reactions still occurred at high RH.

Compared to those on non-haze days, the values of SOR and NOR increased >1.64–2.21 and 2.88–3.33 times during Haze I and II, respectively (Table 1), suggesting greater oxidation of gaseous species and more elevated secondary aerosol formation. These were supported by the higher concentrations of SO_4^{2-} and NO_3^- in Haze I and II. However, in Haze III, the values of SOR and NOR were close to those on non-haze days (Table 1), respectively, and the average SOR and NOR values from 0:00 to 12:00 were only 0.12 and 0.11, respectively. Meanwhile, apparent sharp increases in SO_4^{2-} and NO_3^- concentrations accompanied by high levels of $PM_{2.5}$, SO_2 and NO_2 were observed from 0:00 to 12:00 in Haze III (Fig. 4a, b, c). The high level of SO_2 significantly influenced SOR, but the high RH from 0:00 to 12:00 (average: 77.5%) made

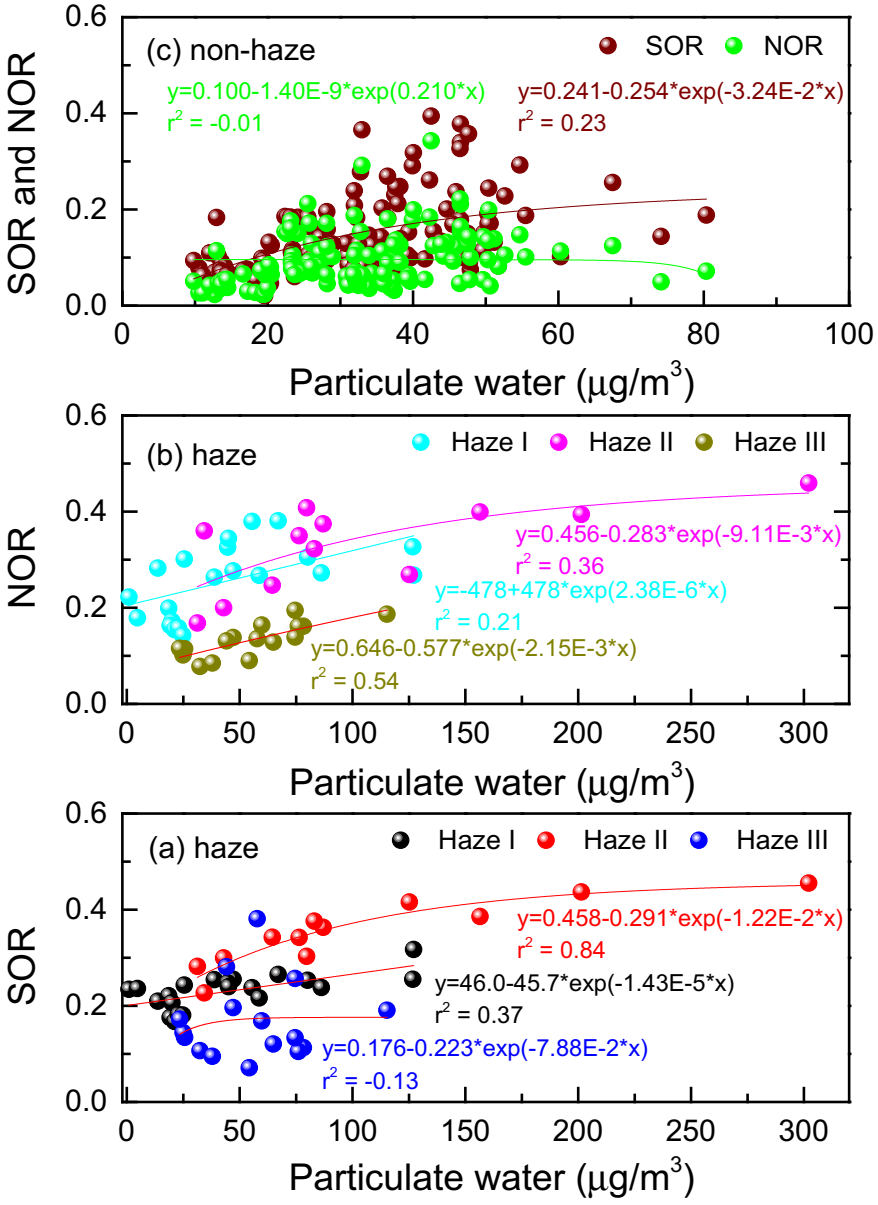

Fig. 7. SOR (a) and NOR (b) under different particulate water content on haze days, and SOR and NOR (c) under different particulate water content on non-haze days in Baoshan district from February 18 to February 28, 2011. The lines in (a), (b) and (c) represent the exponential fits through the data.

more aqueous-phase oxidation of SO_2. All the results demonstrated an important contribution of heterogeneous aqueous oxidation of SO_2 to secondary sulfate aerosols and the elevated SIA concentrations in Haze III (Park et al., 2016). Overall, all the results mentioned above demonstrated different tendencies of the heterogeneous aqueous reactions of SO_2 and NO_2 in the high-nitrate haze episode and the high-sulfate haze episode.

Both gas-phase oxidation and heterogeneous aqueous oxidation can contribute to the formation of sulfate and nitrate from SO_2 and NO_2, and thus increasing the SOR and NOR. Sulfate formation from SO_2 usually takes place by gas-phase reactions with OH (Stockwell and Calvert, 1983), and by heterogeneous reactions with dissolved H_2O_2 or with O_2 under the catalysis of transition metal (Seinfeld and Pandis, 2016). Nitrate formation is also through gas-phase reaction of NO_2 with OH or O_3 during daytime and heterogeneous hydrolysis of N_2O_5 during nighttime (Pathak et al., 2009; Seinfeld and Pandis, 2016). However, gas-phase formation of secondary aerosols is usually expected to decrease during haze episodes. In order to examine the effect of gas-phase oxidation of SO_2 to SO_4^{2-} on haze days, especially the relative roles of photochemistry and heterogeneous aqueous reaction, the exponential correlations of SOR with O_3 in Haze I, II and III were analyzed (Fig. S3). It was found that no obvious correlations existed between SOR and O_3 in Haze II ($r^2 = 0.00$) and III ($r^2 = -0.11$), which suggested that photochemical production had a minor contribution to secondary sulfate, even at high level of O_3 in Haze II (62.3 μg/m^3). In addition, low photochemical oxidation activity in the early morning, represented by a low O_3 concentration, was observed to be accompanied by high levels of $PM_{2.5}$, SO_2 and NO_2 concentrations (Fig. 4c). For Haze II and III, this may be attributed to the high particulate liquid water content in Haze II and the high SO_2 and NO levels in Haze III. These results may indicate that O_3 in Haze II and III could not trigger directly aqueous-phase and gas-phase reactions to produce secondary sulfate particles greatly. Weak correlation between SOR and O_3 was found in Haze I ($r^2 = 0.32$), which suggested the contribution of photochemistry to the secondary sulfate formation. These results may indicate that the contribution of the heterogeneous aqueous reaction became more important for the formation of the secondary inorganic aerosols in high-nitrate haze episodes (Haze I and II).

In addition, field observational evidences show that NO_2 plays a distinct role in the formation of sulfate in the real atmosphere, including surface catalytic reactions of SO_2 and aqueous oxidation of S(IV) under foggy/cloudy conditions with high NH_3 concentration (Wang et al., 2016a; Wang et al.,2016b; Xie et al., 2015). Therefore, the effect of NO_2 on the conversion of SO_2 to sulfate in the haze episodes was examined, and exponential correlation between SOR and NO_2 was calculated (Fig. S3). No correlation in Haze I ($r^2 = -0.07$) and poor correlation in Haze II ($r^2 = 0.12$) were found between SOR and NO_2. However, SOR and NO_2 exhibited a weak correlation in Haze III ($r^2 = 0.33$), which suggested that NO_2 had a weak influence on the conversion of SO_2 to sulfate in Haze III due to the high level of NO_2. As discussed above, gas-phase oxidation of SO_2 by O_3 and/or aqueous-phase oxidation of SO_2 by NO_2 were not important mechanisms of secondary sulfate and nitrate formation on haze days in this study. These results implied the potential complexity of the influence of O_3 and NO_2.

3.3.3. The existing forms of sulfate and nitrate in $PM_{2.5}$ on haze days

More and more high-nitrate haze episodes are observed in China in recent years, and therefore more and more attentions have been paid to the formation of nitrate on haze days. The nitrate formation in the atmosphere is complicated, and there are many factors influencing the formation mechanism of nitrate, such as temperature, RH, ammonium availability, particle acidity, and the preexisting particles (Pathak et al., 2009; Tian et al., 2017). In our study, the average temperature and RH were 7.3 °C and 74.8% on haze days during the sampling period, respectively (Table 1). The high RH contributed to the heterogeneous aqueous reactions of SO_2 and NO_2, especially in high-nitrate haze episodes as discussed above. Meanwhile, high RH could make gaseous HNO_3 and NH_3 be dissolved in humid PM, and hence enhancing particulate NO_3^- and NH_4^+ levels in the atmosphere (Trebs et al., 2004). While the low temperature would contribute to the stability of formed ammonium nitrate because the formed ammonium nitrate is thermodynamically unstable. Considering the existence of heterogeneous aqueous reactions, in this section, the existing forms of sulfate and nitrate in $PM_{2.5}$ on haze days are briefly discussed.

In our study, the regression function between $[NO_3^-]/[SO_4^{2-}]$ and $[NH_4^+]/[SO_4^{2-}]$ on haze days at Baoshan site was:

$$\frac{[NO_3^-]}{[SO_4^{2-}]} = 0.791 \times \frac{[NH_4^+]}{[SO_4^{2-}]} - 1.33 \quad (4)$$

The intercept of the regression line with the axis of $[NH_4^+]/[SO_4^{2-}]$ (*i.e.* the threshold value) was 1.68, indicating that the excess NH_4^+ became available for NO_3^- formation after neutralizing most of the SO_4^{2-} and HSO_4^- when $[NH_4^+]/[SO_4^{2-}] \geq 1.68$. The threshold value was larger than 1.5 and <2.0, indicating that the solid or aqueous NH_4HSO_4 and $NH_4(SO_4)_2$ were the preferred forms of sulfate aerosol phase (Pathak et al., 2009; Squizzato et al., 2013), which was consistent with the result from *in situ* aerosol acidity analysis and with the trend showed in Fig. 8. Fig. 8 shows the nitrate-to-sulfate, *in situ* acidity-to-sulfate and acidity-to-sulfate (molar ratio) as functions of ammonium to sulfate (molar ratio) during the haze days. It can be seen that when $[NH_4^+]/[SO_4^{2-}] < 1.68$, the nitrate-to-sulfate molar ratios ($[NO_3^-]/[SO_4^{2-}]$) were relatively constant but increased dramatically as $[NH_4^+]/[SO_4^{2-}] \geq 1.68$. This suggested that nitrate would be formed *via* gas-phase reaction $HNO_3(g) + NH_3(g) \leftrightharpoons NH_4NO_3(s, aq)$ when $[NH_4^+]/[SO_4^{2-}] \geq 1.68$. In addition, the neutralization of acidity also showed similar characteristics. As shown in Fig. 8, the $[H^+]_{Ins}/[SO_4^{2-}]$ and $[H^+]_{Total}/[SO_4^{2-}]$ ratios showed a sharp decrease when $[NH_4^+]/[SO_4^{2-}] < 1.68$. These clearly indicated that the neutralization of *in situ* acidity by ambient ammonia ($[H^+]_{Ins} + NH_3 \rightarrow NH_4^+$) was the principal pathway until $[NH_4^+]/[SO_4^{2-}]$ ratio reached 1.68. However, when $[NH_4^+]/[SO_4^{2-}] \geq 1.68$, the neutralization of acidity was almost stopped and the $[H^+]_{Ins}/[SO_4^{2-}]$ was negligible. The negligible $[H^+]_{Ins}/[SO_4^{2-}]$ indicated that almost all the *in situ* acidity was neutralized before $[NH_4^+]/[SO_4^{2-}] = 1.68$, but there still existed some un-neutralized acid in total acid, which is consistent with previous studies (Huang et al., 2011). In addition, Excess NH_4^+ was defined as $[NH_4^+]_{excess} = ([NH_4^+]/[SO_4^{2-}]\text{-}1.68) \times [SO_4^{2-}]$. The calculated concentrations of excess NH_4^+ were always higher than 0. Significant linear correlations in Haze I ($y = 0.716x + 0.0125$, $r^2 = 0.99$) and Haze III ($y = 0.430x + 0.0488$, $r^2 = 0.69$) as well as weak correlation in Haze II ($y = 0.392x + 0.177$, $r^2 = 0.29$) were found between the excess NH_4^+ and NO_3^-, which also indicated ammonium nitrate formation *via* gas-phase reaction between HNO_3 and NH_3 to different degrees, especially in Haze I and III. It should be pointed out that all the slopes in the haze days were smaller than 1, which isn't consistent with the molar ratio for the reaction between HNO_3 and NH_3, indicating that there were still some of excess NH_4^+ ions bounded to species other than NO_3^-, or some heterogeneous reactions resulting in the formation of nitrate occurred without involving NH_3, such as heterogeneous hydrolysis of N_2O_5 during nighttime and heterogeneous conversion of NO_2 on mineral dust (Pathak et al., 2009; Seinfeld and Pandis, 2016).

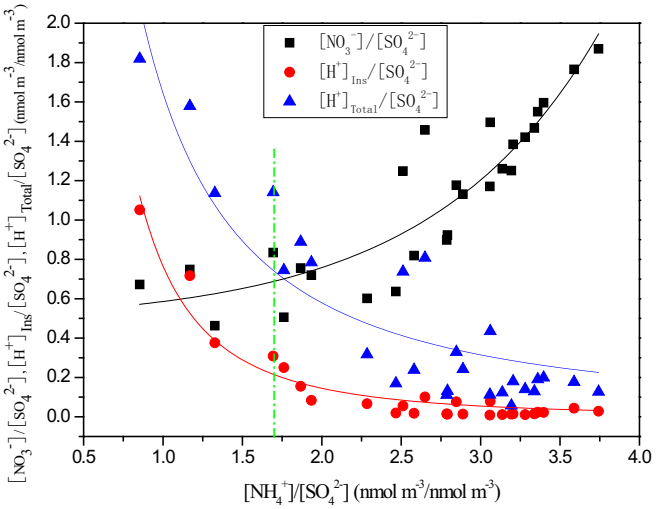

Fig. 8. Nitrate-to-sulfate, *in situ* acidity-to-sulfate and acidity-to-sulfate (molar ratio) as functions of ammonium to sulfate (molar ratio) during haze days.

4. Conclusion

During the selected study period, three haze episodes occurred, and fine particle pollution in Baoshan was serious on haze days. The average mass concentration value of the $PM_{2.5}$ on haze days (79.4 μg/m^3) was 1.86 times higher than that on non-haze days (42.6 μg/m^3), and the highest concentration even reached to 199 μg/m^3. The high SIA concentrations and the higher SOR and NOR on haze days indicated that enhanced conversions from SO_2 and NO_x to their corresponding particulate phases, and the formation of the continuous haze episodes mainly originated from the secondary pollution. While secondary pollution could be ascribed to local pollution and regional transport impact. The formation of Haze I and Haze II was associated with the long-range transport of air pollutants and local secondary pollution, whereas the occurrence of Haze III was a combined result of local secondary pollution and intra-regional transport of SIA. Moreover, the high-nitrate haze episode and the high-sulfate haze episode during the study period were identified. Further simulations revealed that the $PM_{2.5}$ particles had strong acidity during the high-nitrate and high-sulfate haze episodes whether they were calculated by E-AIM 4 or by ISORROPIA II. It was also found that particulate liquid water was more sensitive to nitrate than sulfate, and played significant roles in the heterogeneous aqueous reactions of NO_2 and secondary nitrate formation during haze episodes, especially in the high-sulfate haze episode. Further analysis indicated that the high-nitrate haze episode favoured the occurrence

of heterogeneous aqueous phase oxidation of SO_2, and the more water in the particles, the more SO_2 conversion. No obvious correlation between SOR and particulate liquid water in the high-sulfate haze episode presented an evidence for more aqueous-phase oxidation of SO_2 due to the higher average RH, the higher levels of SO_2 and NO_x, and the higher concentrations of hygroscopic SO_4^{2-} and NO_3^-, as well as the consistently lower SOR. Although more cases are needed for further confirmation, this work provides an important field measurement-based evidence for understanding the important contributions of the heterogeneous aqueous reactions to secondary aerosols and the tendencies of heterogeneous aqueous reactions in the formation of secondary sulfate and nitrate aerosols in suburban Shanghai.

Disclaimer

The authors declare no competing financial interest.

Acknowledgements

This work was supported by the National Key R & D Program of China (2017YFC0209505) and the National Natural Science Foundation of China (Grant Nos. 21777027, 41475110 and 21277028).

Appendix A. Supplementary data

Supplementary data to this article can be found online at https://doi.org/10.1016/j.scitotenv.2018.04.086.

References

Andreae, M.O., Schmid, O., Yang, H., Chand, D., Yu, J.Z., Zeng, L., Zhang, Y., 2008. Optical properties and chemical composition of the atmospheric aerosol in urban Guangzhou, China. Atmos. Environ. 42, 6335–6350.

Arimoto, R., Duce, R.A., Savoie, D.L., Prospero, J.M., Talbot, R., Cullen, J.D., et al., 1996. Relationships among aerosol constituents from Asia and the North Pacific during PEM-West A. J. Geophys. Res. 101, 2011–2023.

Bougiatioti, A., Nikolaou, P., Stavroulas, I., Kouvarakis, G., Weber, R., Nenes, A., et al., 2016. Particle water and pH in the eastern Mediterranean: source variability and implications for nutrient availability. Atmos. Chem. Phys. 16, 4579–4591.

Cheng, H., Gong, W., Wang, Z., Zhang, F., Wang, X., Lv, X., et al., 2014. Ionic composition of submicron particles ($PM_{1.0}$) during the long-lasting haze period in January 2013 in Wuhan, Central China. J. Environ. Sci. 26, 810–817.

Clegg, S.L., Brimblecombe, P., Wexler, A.S., 1998. Thermodynamic model of the system H^+-NH_4^+-SO_4^{2-}-NO_3^--H_2O at tropospheric temperatures. J. Phys. Chem. A 102, 2137–2154.

Deng, H., Tan, H., Li, F., Cai, M., Chan, P.W., Xu, H., et al., 2016. Impact of relative humidity on visibility degradation during a haze event: a case study. Sci. Total Environ. 569-570, 1149–1158.

Ding, X.X., Kong, L.D., Du, C.T., Zhanzakova, A., Fu, H.B., Tang, X.F., et al., 2017. Characteristics of size-resolved atmospheric inorganic and carbonaceous aerosols in urban Shanghai. Atmos. Environ. 167, 625–641.

Du, H., Kong, L., Cheng, T., Chen, J., Du, J., Li, L., et al., 2011. Insights into summertime haze pollution events over Shanghai based on online water-soluble ionic composition of aerosols. Atmos. Environ. 45, 5131–5137.

Fountoukis, C., Nenes, A., 2007. ISORROPIA II: a computationally efficient thermodynamic equilibrium model for K^+–Ca^{2+}–Mg^{2+}–NH_4^+–Na^+–SO_4^{2-}–NO_3^-–Cl^-–H_2O aerosols. Atmos. Chem. Phys. 7, 4639–4659.

Friese, E., Ebel, A., 2010. Temperature dependent thermodynamic model of the system H^+-NH_4^+-Na^+-SO_4^{2-}-NO_3^--Cl^--H_2O. J. Phys. Chem. A 114, 11595–11631.

Fu, H., Chen, J., 2017. Formation, features and controlling strategies of severe haze-fog pollutions in China. Sci. Total Environ. 578, 121–138.

Guo, S., Hu, M., Zamora, M.L., Peng, J., Shang, D., Zheng, J., et al., 2014. Elucidating severe urban haze formation in China. Proc. Natl. Acad. Sci. U. S. A. 111, 17373–17378.

Guo, H., Sullivan, A.P., Campuzano-Jost, P., Schroder, J.C., Lopez-Hilfiker, F.D., Dibb, J.E., et al., 2016. Fine particle pH and the partitioning of nitric acid during winter in the northeastern United States. J. Geophys. Res.-Atmos. 121, 10355–10376.

Han, B., Zhang, R., Yang, W., Bai, Z., Ma, Z., Zhang, W., 2016. Heavy haze episodes in Beijing during January 2013: inorganic ion chemistry and source analysis using highly time-resolved measurements from an urban site. Sci. Total Environ. 544, 319–329.

Hodas, N., Sullivan, A.P., Skog, K., Keutsch, F.N., Collett Jr., J.L., Decesari, S., et al., 2014. Aerosol liquid water driven by anthropogenic nitrate: implications for lifetimes of water-soluble organic gases and potential for secondary organic aerosol formation. Environ. Sci. Technol. 48, 11127–11136.

Hoyle, C.R., Fuchs, C., et al., 2016. Aqueous phase oxidation of sulphur dioxide by ozone in cloud droplets. Atmos. Chem. Phys. 16, 1693–1712.

Hua, Y., Cheng, Z., Wang, S., Jiang, J., Chen, D., Cai, S., et al., 2015. Characteristics and source apportionment of $PM_{2.5}$ during a fall heavy haze episode in the Yangtze River Delta of China. Atmos. Environ. 123, 380–391.

Huang, X., Qiu, R., Chan, C.K., Ravi Kant, P., 2011. Evidence of high $PM_{2.5}$ strong acidity in ammonia-rich atmosphere of Guangzhou, China: transition in pathways of ambient ammonia to form aerosol ammonium at $[NH_4^+]/[SO_4^{2-}] = 1.5$. Atmos. Res. 99, 488–495.

Huang, R.J., Zhang, Y., Bozzetti, C., Ho, K.F., Cao, J.J., Han, Y., et al., 2014. High secondary aerosol contribution to particulate pollution during haze events in China. Nature 514, 218–222.

Kong, L., Yang, Y., Zhang, S., Zhao, X., Du, H., Fu, H., et al., 2014. Observations of linear dependence between sulfate and nitrate in atmospheric particles. J. Geophys. Res. Atmos. 119, 341–361.

Laskin, J., Laskin, A., Roach, P.J., Slysz, G.W., Anderson, G.A., Nizkorodov, S.A., et al., 2010. High-resolution desorption electrospray ionization mass spectrometry for chemical characterization of organic aerosols. Anal. Chem. 82, 2048–2058.

Li, G., Bei, N., Cao, J., Huang, R., Wu, J., Feng, T., et al., 2017. A possible pathway for rapid growth of sulfate during haze days in China. Atmos. Chem. Phys. 17, 3301–3316.

Liu, Z., Hu, B., Zhang, J., Yu, Y., Wang, Y., 2016. Characteristics of aerosol size distributions and chemical compositions during wintertime pollution episodes in Beijing. Atmos. Res. 168, 1–12.

Liu, M., Song, Y., Zhou, T., Xu, Z., Yan, C., Zheng, M., et al., 2017. Fine particle pH during severe haze episodes in northern China. Geophys. Res. Lett. 44, 5213–5221.

Ma, Q., Wu, Y., Zhang, D., Wang, X., Xia, Y., Liu, X., et al., 2017. Roles of regional transport and heterogeneous reactions in the $PM_{2.5}$ increase during winter haze episodes in Beijing. Sci. Total Environ. 599–600, 246–253.

Nenes, A., Pandis, S.N., Pilinis, C., 1998. ISORROPIA: a new thermodynamic equilibrium model for multiphase multicomponent inorganic aerosols. Aquat. Geochem. 4, 123–152.

Park, S.S., Kim, Y.J., 2004. $PM_{2.5}$ particles and size-segregated ionic species measured during fall season in three urban sites in Korea. Atmos. Environ. 38, 1459–1471.

Park, S.S., Cho, S.Y., Jung, C.H., Lee, K.H., 2016. Characteristics of water-soluble inorganic species in PM_{10} and $PM_{2.5}$ at two coastal sites during spring in Korea. Atmos. Pollu. Res. 7, 370–383.

Parworth, C.L., Young, D.E., Kim, H., Zhang, X., Cappa, C.D., Collier, S., Zhang, Q., 2017. Wintertime water-soluble aerosol composition and particle water content in Fresno, California. J. Geophys. Res.-Atmos. 122, 3155–3170.

Pathak, R.K., Wu, W.S., Wang, T., 2009. Summertime $PM_{2.5}$ ionic species in four major cities of China: Nitrate formation in an ammonia-deficient atmosphere. Atmos. Chem. Phys. 9, 1711–1722.

Putaud, J.P., Raes, F., Van Dingenen, R., Bruggemann, E., Facchini, M.C., Decesari, S., et al., 2004. European aerosol phenomenology-2: chemical characteristics of particulate matter at kerbside, urban, rural and background sites in Europe. Atmos. Environ. 38, 2579–2595.

Qiao, T., Zhao, M., Xiu, G., Yu, J., 2015. Seasonal variations of water soluble composition (WSOC, Hulis and WSIIs) in PM_1 and its implications on haze pollution in urban Shanghai, China. Atmos. Environ. 123, 306–314.

Qiao, T., Zhao, M., Xiu, G., Yu, J., 2016. Simultaneous monitoring and compositions analysis of PM_1 and $PM_{2.5}$ in Shanghai: implications for characterization of haze pollution and source apportionment. Sci. Total Environ. 557-558, 386–394.

Quan, J., Liu, Q., Li, X., Gao, Y., Jia, X., Sheng, J., et al., 2015. Effect of heterogeneous aqueous reactions on the secondary formation of inorganic aerosols during haze events. Atmos. Environ. 122, 306–312.

QX_T113, 2010. Observation and Forecasting Levels of Haze (in Chinese).

Seinfeld, J.H., Pandis, S.N., 2016. Atmospheric Chemistry and Physics: From Air Pollution to Climate Change. Third ed. John Wiley & Sons, Inc., Hoboken, New Jersey.

Squizzato, S., Masiol, M., Brunelli, A., Pistollato, S., Tarabotti, E., Rampazzo, G., et al., 2013. Factors determining the formation of secondary inorganic aerosol: a case study in the Po Valley (Italy). Atmos. Chem. Phys. 13, 1927–1939.

Stockwell, W.R., Calvert, J.G., 1983. The mechanism of the HO-SO_2 reaction. Atmos. Environ. 17, 2231–2235.

Sun, Y., Zhuang, G., Tang, A., Wang, Y., An, Z., 2006. Chemical characteristics of $PM_{2.5}$ and PM_{10} in haze-fog episodes in Beijing. Environ. Sci. Technol. 40, 3148–3155.

Tian, M., Wang, H., Chen, Y., Zhang, L., Shi, G., Liu, Y., et al., 2017. Highly time-resolved characterization of water-soluble inorganic ions in $PM_{2.5}$ in a humid and acidic mega city in Sichuan Basin, China. Sci. Total Environ. 580, 224–234.

Trebs, I., Meixner, F.X., Slanina, J., Otjes, R., Jongejan, P., Andreae, M.O., 2004. Real-time measurements of ammonia, acidic trace gases and water-soluble inorganic aerosol species at a rural site in the Amazon Basin. Atmos. Chem. Phys. 4, 967–987.

Wang, W., Primbs, T., Tao, S., Zhu, T., Simonich, S.L.M., 2009. Atmospheric particulate matter pollution during the 2008 Beijing Olympics. Environ. Sci. Technol. 43, 5314–5320.

Wang, X., Wang, W., Yang, L., Gao, X., Nie, W., Yu, Y., Xu, P., Zhou, Y., Wang, Z., 2012. The secondary formation of inorganic aerosols in the droplet mode through heterogeneous aqueous reactions under haze conditions. Atmos. Environ. 63, 68–76.

Wang, J., Hu, Z., Chen, Y., Chen, Z., Xu, S., 2013. Contamination characteristics and possible sources of PM_{10} and $PM_{2.5}$ in different functional areas of Shanghai, China. Atmos. Environ. 68, 221–229.

Wang, M., Cao, C., Li, G., Singh, R.P., 2015. Analysis of a severe prolonged regional haze episode in the Yangtze River Delta, China. Atmos. Environ. 102, 112–121.

Wang, G., Zhang, R., Gomez, M.E., Yang, L., Zamora, M.L., Hu, M., et al., 2016a. Persistent sulfate formation from London Fog to Chinese haze. Proc. Natl. Acad. Sci. U. S. A. 113, 13630–13635.

Wang, H.L., Qiao, L.P., Lou, S.R., Zhou, M., Ding, A.J., Huang, H.Y., et al., 2016b. Chemical composition of $PM_{2.5}$ and meteorological impact among three years in urban Shanghai, China. J. Clean. Prod. 112, 1302–1311.

Whiteaker, J.R., Suess, D.T., Prather, K.A., 2002. Effects of meteorological conditions on aerosol composition and mixing state in Bakersfield, CA. Environ. Sci. Technol. 36, 2345–2353.

Xiang, P., Zhou, X., Duan, J., Tan, J., He, K., Yuan, C., et al., 2017. Chemical characteristics of water-soluble organic compounds (WSOC) in $PM_{2.5}$ in Beijing, China: 2011–2012. Atmos. Res. 183, 104–112.

Xie, Y., Ding, A., Nie, W., Mao, H., Qi, X., Huang, X., et al., 2015. Enhanced sulfate formation by nitrogen dioxide: implications from in situ observations at the SORPES station. J. Geophys. Res. Atmos. 120 (12) (679-12,694).

Xue, J., Griffith, S.M., Yu, X., Lau, A.K.H., Yu, J.Z., 2014. Effect of nitrate and sulfate relative abundance in $PM_{2.5}$ on liquid water content explored through half-hourly observations of inorganic soluble aerosols at a polluted receptor site. Atmos. Environ. 99, 24–31.

Yang, Y.R., Liu, X.G., Qu, Y., An, J.L., Jiang, R., Zhang, Y.H., et al., 2015. Characteristics and formation mechanism of continuous hazes in China: a case study during the autumn of 2014 in the North China Plain. Atmos. Chem. Phys. 15, 8165–8178.

Yao, X.H., Chan, C.K., Fang, M., Cadle, S., Chan, T., Mulawa, P., et al., 2002. The water-soluble ionic composition of $PM_{2.5}$ in Shanghai and Beijing, China. Atmos. Environ. 36, 4223–4234.

Yao, L., Yang, L., Chen, J., Wang, X., Xue, L., Li, W., et al., 2016. Characteristics of carbonaceous aerosols: impact of biomass burning and secondary formation in summertime in a rural area of the North China Plain. Sci. Total Environ. 557–558, 520–530.

Yin, Z., Wang, H., 2017. Role of atmospheric circulations in haze pollution in December 2016. Atmos. Chem. Phys. 17, 11673–11681.

Zhang, Q., Jimenez, J.L., Worsnop, D.R., Canagaratna, M., 2007. A case study of urban particle acidity and its influence on secondary organic aerosol. Environ. Sci. Technol. 41, 3213–3219.

Zhao, M., Huang, Z., Qiao, T., Zhang, Y., Xiu, G., Yu, J., 2015a. Chemical characterization, the transport pathways and potential sources of $PM_{2.5}$ in Shanghai: seasonal variations. Atmos. Res. 158-159, 66–78.

Zhao, M., Qiao, T., Huang, Z., Zhu, M., Xu, W., Xiu, G., Tao, J., Lee, S., 2015b. Comparison of ionic and carbonaceous compositions of $PM_{2.5}$ in 2009 and 2012 in Shanghai, China. Sci. Total Environ. 536, 695–703.

Zheng, G.J., Duan, F.K., Su, H., Ma, Y.L., Cheng, Y., Zheng, B., et al., 2015. Exploring the severe winter haze in Beijing: the impact of synoptic weather, regional transport and heterogeneous reactions. Atmos. Chem. Phys. 15, 2969–2983.